VERSITA
Studia Geotechnica et Mechanica, Vol. XXXV, No. 4, 2013
DOI: 10.2478/sgem-2013-0034

STEADY STATE OF SOLID-GRAIN INTERFACES DURING SIMULATED CPT

JOANNA BUTLANSKA, MARCOS ARROYO, ANTONIO GENS

Universitat Politècnica de Catalunya, BarcelonaTECH,
Department of Geotechnical Engineering, Barcelona, Spain,
e-mail: joanna.butlanska@upc.edu, marcos.arroyo@upc.edu, antonio.gens@upc.edu

Abstract: It has recently been shown (Arroyo et al. [1]) that 3D DEM models are able to reproduce with reasonable accuracy the macroscopic response of CPT performed in calibration chambers filled with sand. However, the cost of each simulation is an important factor. Hence, to achieve manageable simulation times the discrete material representing the sand was scaled up to sizes that were more typical of gravel than sand. A side effect of the scaled-up discrete material size employed in the model was an increased fluctuation of the macro-response that can be filtered away to observe a macroscopic steady-state cone resistance. That observation is the starting point of this communication, where a series of simulations in which the size ratio between penetrometer and particles is varied are systematically analyzed. A micromechanical analysis of the penetrometer–particle interaction is performed. These curves reveal that a steady state is arrived also at the particle–cone contact level. The properties of this dynamic interface are independent of the initial density of the granular material.

1. INTRODUCTION

Increases in computing power have made the simulation of geotechnical boundary value problems with DEM an attractive possibility. One problem where this type of simulation might be helpful is cone penetration. Arroyo et al. [1] validated this approach, showing that 3D DEM models of CPT in a calibration chamber resulted in cone point resistance values in close agreement with predictions based in physical models. Several aspects of this type of models have been explored further by Butlanska et al. [3], Butlanska et al. [4], McDowell et al. [11], Lin and Wu [8] and Arroyo et al. [2].

DEM models can be examined at various levels of resolution, whereby it is convenient to distinguish between the micro-scale, the meso-scale and the macro-scale. The macro-scale deals with system responses of direct engineering interest, for instance, cone tip resistance in the CPT problem. The micro-scale level of resolution describes variables at the highest possible resolution, that is, at the particle or contact level. In between, meso-scale descriptions are based on averaging volumes and can be related to classical continuum descriptions of the problem.

One interesting aspect of DEM simulations of geotechnical problems still being explored is the effect of boundary conditions on the problem outcomes. Marketos and Bolton [10] showed how the apparent macroscale stiffness of an oedometric test could

be strongly affected by the microscale details of the contact at the boundary top and bottom walls. For axisymmetric problems, Cui et al. [6] and Arroyo et al. [2] have shown that rigid walls enforcing symmetry conditions induce specific microstructural features and result in changes of macroscopic response. That research deals with pre-existing boundaries, i.e., boundaries that are in place when the model is built. The insertion of the CPT creates new rigid boundaries within the granular media. Here we explore some microscale features of that newly created boundary and put them in relation with the macro response.

2. NUMERICAL MODEL

2.1. NUMERICAL APPROACH

The DEM PFC3D code (Itasca [9]) was used to perform all numerical simulations mentioned in this paper. The code is a simplified version of the discrete element method proposed by Cundall et al. [7]. The model is composed of spherical particles that displace independently of one another and only interact at the contact point. The particles are assumed rigid and cannot rotate. The contact law employed is lineal elasto-plastic. The normal and tangential stiffness (k_n and k_s) at any contact are calculated using the following scaling rule

$$\begin{aligned} k_n &= 2K_{\text{eff}} \frac{D_1 D_2}{D_1 + D_2}, \\ k_s &= \alpha k_n, \end{aligned} \tag{1}$$

where α and K_{eff} are parameters to be calibrated. The interparticle friction (φ_μ) describes the plastic part of the contact law. To speed up model convergence a non-viscous damping (δ) was also included.

2.2. CALIBRATION METHOD

The model calibration was performed on a small sample with 8 mm side and filled with approximately 4700 particles with the grain distribution shown in Fig. 1 (DEM calibration). The sample was prepared using the radius expansion method (REM). Material parameters (K_{eff}, α, φ_μ and δ) were determined by trial and error in order to provide a best fit to a single isotropically compressed drained triaxial test confined at 100 kPa and formed with D_R = 75%. The best fit was found for: K_{eff} = 300 MN, α = 0.25, tan(φ_μ) = 0.35 and δ = 0.05 (Butlanska et al. [5]).

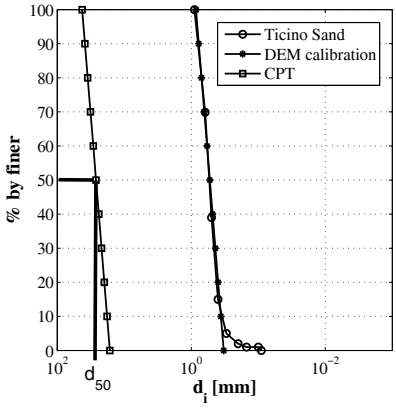

Fig. 1. Grain size curves of Ticino sand used in numerical simulations

2.3. CALIBRATION CHAMBER AND CONE DEVICE

A schematic view of the calibration chamber and cone devices used in the simulations can be seen in Fig. 2. The calibration chamber was designed as cylindrical with rigid, frictionless walls. The diameter (D_{cc}) and height (H_{cc}) of CC were 1.2 m and 0.7 m, respectively. Moreover, the CC was filled with approximately 60 000 particles with a grain size distribution as shown in Fig. 1 (CPT). Four different cone tip sizes were used. The cone tip in all cases had an angle of 60 degrees and was frictional. Perfect roughness was assumed in the contact between cone and particles.

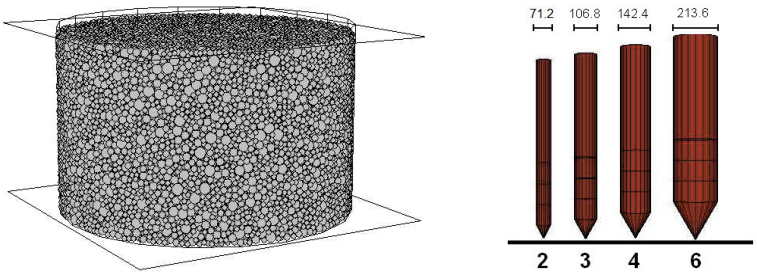

(a) VCC (b) Cone tips

Fig. 2. View of (a) calibration chamber and (b) four different cone sizes used in the analysis

2.4. TESTING PROGRAM

Two deep penetration test series were performed at two different initial relative densities (75.2 and 90.7%). Each series included one test with each different cone tip sizes. The CPTs were performed under stress-controlled radial and top boundary con-

ditions (BC1), maintaining 100 kPa in all the controlled boundaries. All CPTs were analyzed to a maximum penetration depth of 0.6 m. The characteristics of the numerical models in the simulation program are summarized in Table 1.

Table 1

Characteristics of numerical model and simulation program

Set	Test ID	d_c (mm)	h_c (mm)	R_d (–)	n_p (–)	σ_{v0} (kPa)	σ_{r0} (kPa)	D_R (%)	BC (–)	OCR (–)
Set 1	T16	71.2	62	16.8	2.69	100	100	75.2	1	1
	T25	106.8	92	11.2	4.03					
	T26	142.4	123	8.4	5.37					
	T27	213.6	185	5.6	8.06					
Set 2	T20	71.2	62	16.8	2.69			90.7		
	T29	106.8	92	11.2	4.03					
	T30	142.4	123	8.4	5.37					
	T31	213.6	185	5.6	8.06					

d_c – diameter of cone tip, h_c – height of cone tip,
R_d – relative size of the chamber (D_{cc}/d_c), n_p – relative particle size (d_c/d_{50}),
BC – boundary conditions (σ_v = const and σ_h = const),
OCR – overconsolidated ratio

2.5. INITIAL STATE

The initial state of the specimens is attained by a process involving random seeding, radius expansion method and servo-controlled imposition of the target initial stress and density. To evaluate possible inhomogeneity within the specimen (Butlanska et al. [3]) the initial state of the calibration chamber was assessed by (i) the observation of normal contact force networks developed between particles (Fig. 3), (ii) the measure of the total number of contacts in the chamber, the magnitude of normal and tangential contact forces (Fig. 4), and (iii) the examination of the mesoscopic values of porosity (n), coordination number (C_N) and stresses (σ_{ii}) along the axis of symmetry (Fig. 5).

Looking at the normal contact force networks developed between contacting particles (Fig. 3) a visible difference between medium-dense and very-dense specimens is observed. For the medium-dense sample an arched pattern of very small normal contact forces ($<F_{n,\mathrm{mean}}$) close to the radial and bottom walls can be seen. Moreover, in both specimens loose zones along the axis of symmetry are observed. The porosity and coordination number distributions shown in Fig. 5(a) and Fig. 5(b) confirm these observations.

The orientation of the contacts shown in Fig. 4(a) is quite isotropic. The maximum number of contacts measured in a given direction is 24 at D_R = 75.2% and 30 at D_R = 90.7%. The magnitude of normal and tangential contact forces (Fig. 4b and Fig. 4c) is also isotropic.

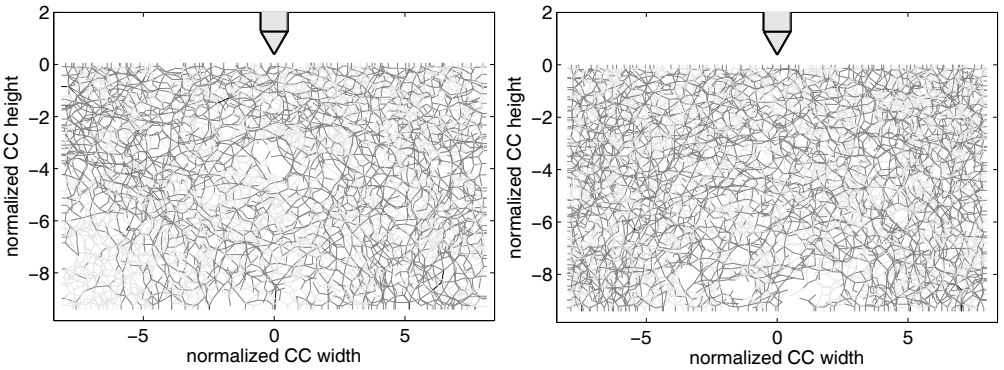

DR = 75.2% (T16, T25, T26, T27) DR = 90.7% (T20, T29, T30, T31)

Fig. 3. Contact normal forces for particles lying within a vertical section of the chamber. Forces exceeding average normal force are plotted in black and forces smaller than the average force are plotted in gray. The lines join the centroids of contacting spheres. The line thickness is proportional to the magnitude of the normal force

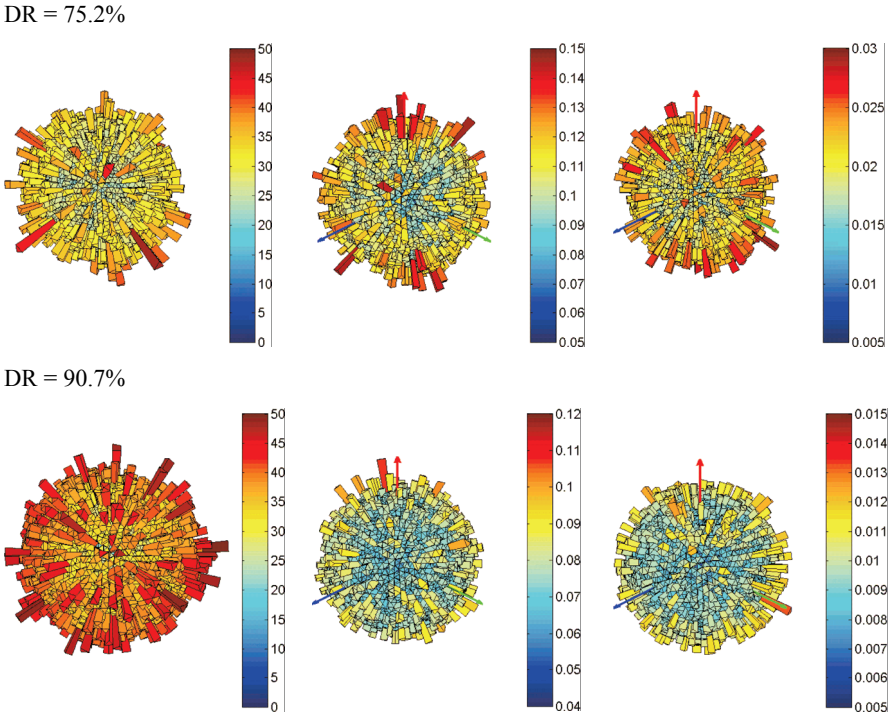

(a) N_c (b) F_n (c) F_t

Fig. 4. Contact (a) orientation, (b) magnitude of normal forces and (c) magnitude of tangential forces in the calibration chamber at initial stage

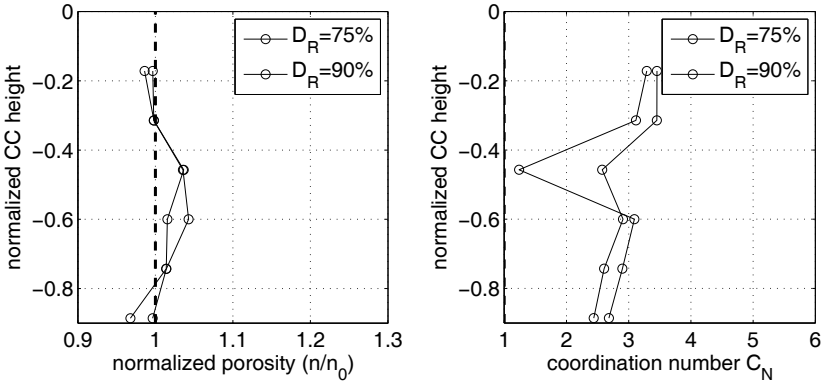

(a) porosity (b) coordination number

(c) radial stress (d) vertical stress

Fig. 5. Mesoscopic values calculated in cylindrical shells of outer radius $2D_{50}$ around the axis of symmetry (dashed line represents target value)

The effect of the rigid wall is also observed (Fig. 5) and resulted in either an increased stress or density (servo controlled wall: radial and top walls) or decreased stress and density (fixed wall: top wall).

3. SIMULATION RESULTS

3.1. MACROSCOPIC STEADY STATE

At the macro-level, the main results are the raw penetration or q_c vs. h_p curves (Fig. 6). The main effect that is visible in these test series is that increased cone sizes result in reduced cone resistances. This is a size effect that can be explained, almost

exclusively, by the relative cone-chamber size, R_D (Table 1). This aspect is examined in detail by Butlanska et al. [4] and will not be treated in here.

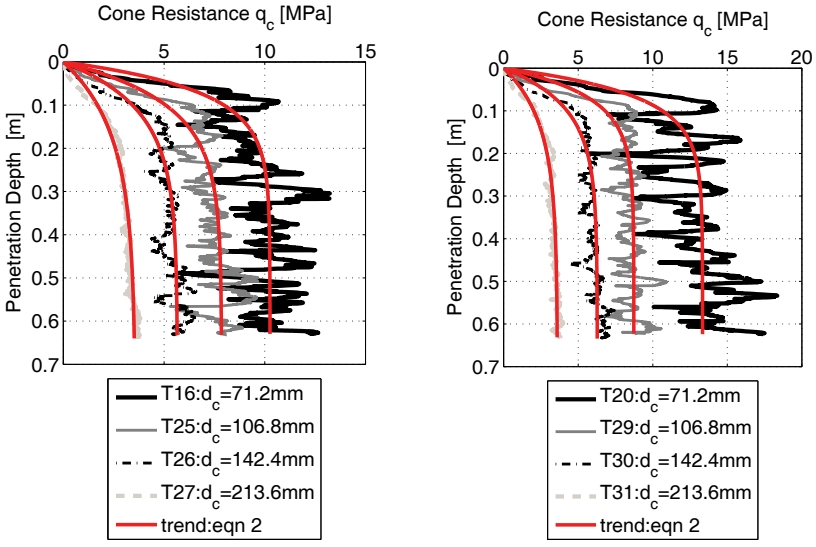

(a) D_R = 75% (b) D_R = 90%

Fig. 6. View of penetrograms: q_c vs. h_p for different cone tip sizes for (a) *DR* = 75% and (b) DR = 90%

It can also be observed that as the ratio between cone size and mean particle size, n_p, increases (d_c increases) there is a visible smoothing of the penetration curves with much smaller oscillations of the cone tip resistance values. This proves that these oscillations appearing in the graph can be treated as a noise artifact of the scaled-up discrete material. To filter that noise the following trend line is fitted to the raw penetration curves (Arroyo et al. [1]),

$$q_{c,\text{trend}}(h_p) = a[1-\exp(-bh_p)] \tag{2}$$

where $q_{c,\text{trend}}$ (MPa) is a cone resistance, h_p is a penetration depth and a and b are fitting parameters. Parameter a (MPa) gives the asymptotic or steady state value of cone resistance; whereas parameter b (1/m) is inversely related to the onset of the steady state. For instance, calling $h_{SS(\text{macro})}$, the depth at which 95% of the steady state value is reached, then

$$h_{SS(\text{macro})} \approx \frac{3}{b}. \tag{3}$$

The relevant results are collected in Table 2. As can be seen the fitting is better (larger R^2) for the smaller cones, a consequence of the smoother oscillation. The steady state depth for the macro response is increasing with cone size and decreasing somewhat with relative density.

Table 2

Main macro-level results

Set	Test ID	a (MPa)	b (1/m)	R^2 (–)	$h_{SS(macro)}$ (mm)	$h_{SS(macro)}/d_c$ (–)
Set 1	T16	10.36	15	0.622	200	2.8
	T25	7.72	10.4	0.784	288	2.8
	T26	5.73	9.3	0.844	322	2.3
	T27	3.42	6.4	0.951	469	2.2
Set 2	T20	12.97	16	0.415	188	2.6
	T29	8.82	15.1	0.725	199	1.9
	T30	6.22	11.3	0.865	265	1.9
	T31	3.67	8.2	0.942	366	1.7

3.2. MICROSCOPIC STEADY STATE

The development of microstructure at the cone interface is explored plotting the number of particles in contact with the cone tip, N_c, as a function of cone tip penetration (Fig. 7). The main feature of these plots is that they show two clearly marked phases: the number of particles in contact with the cone tip increases and then oscillates around a constant mean value (μ_c), in what can be seen as a microscopic steady state zone. The mean contact value and its coefficient of variation for each test are tabulated in Table 3. All the characteristic values of this microscopic steady state appear to be independent of the initial density of the granular material filling the chamber.

The initial zone of increasing contacts corresponds to the cone tip entering the granular media. The microscopic steady state starts slightly before the cone tip has been fully pushed inside, which, for a cone angle of 60°, happens when $h_p = 1.15\, d_c$. It is then clear that a microscopic steady state precedes the onset of the macroscopic one.

The steady state particle number μ_c naturally increases with cone size. To appreciate if any size effect is present, a non-dimensional measure of particle contact density at the interface is evaluated. This interface contact density (ICD) is obtained as the ratio of cone surface (A_c) to mean projected particle area (A_{D50} the section of a D_{50} particle) divided by the number of contacts,

$$\mathrm{ICD} = \frac{A_c}{\mu_c A_{D50}} = \frac{n_p^2}{\mu_c \cos\alpha}. \tag{4}$$

It appears that this normalized interface contact density increases slightly with cone size, scaling approximately with the cubic root of cone diameter. It is interesting to note that a smaller ICD does not affect the ability to sustain large forces in this non-crushable material, as indicated by the mean contact force value ($F_{av} = a/\mu_c$) at steady state.

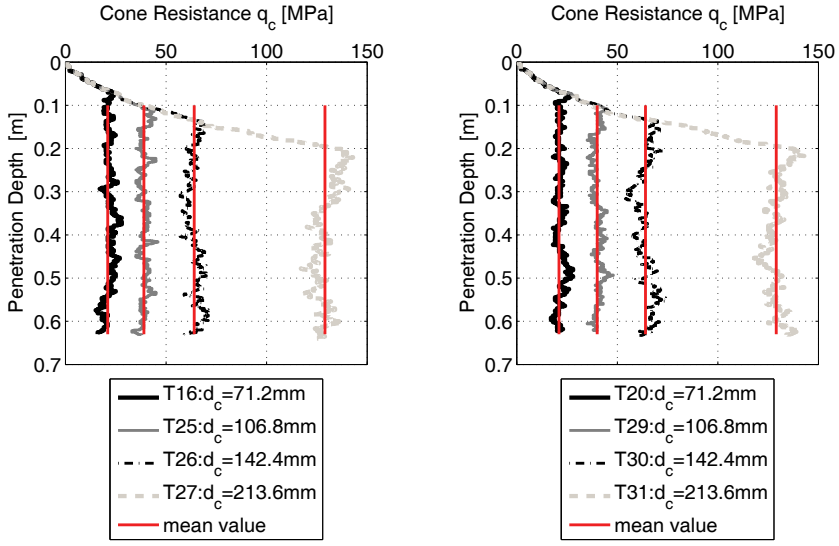

(a) (b)

Fig. 7. View of cone-particles contacts for different cone tip sizes for (a) D_R = 75% and (b) D_R = 90%

Table 3

Main micro-level results

Set	Test ID	μ_c	σ	CV	$h_{SS(micro)}$	$h_{SS(micro)}/d_c$	ICD	F_{av}
		(–)	(–)	(%)	(mm)	(–)	(–)	kN
Set 1	T16	21	2.33	11.1	71	0.99	0.7	4.0
	T25	39	2.32	6.0	114	1.07	0.8	3.5
	T26	64	3.35	5.2	137	0.96	0.9	2.9
	T27	129	5.39	4.2	211	0.98	1.0	1.9
Set 2	T20	21	2.13	10.2	75	1.05	0.7	5.0
	T29	40	2.23	5.6	108	1.01	0.8	4.0
	T30	64	4.09	6.4	135	0.95	0.9	3.1
	T31	129	4.66	3.6	202	0.94	1.0	2.0

4. CONCLUSIONS

Macroscopic steady states such as those observed in these simulations are a common occurrence in physical calibration chamber testing. It is much harder to observe the nature of the microscopic arrangement of the granular material around the penetrating cone. DEM offers with relative ease that kind of insight. The fact that the steady state cone contact values are independent of the initial specimen density does indicate that a granular flow takes place around the cone tip during insertion. This opens the door for a deeper understanding of CPT usage in problems where granular flow dynamics are important.

ACKNOWLEDGMENTS

The support of the Ministry of Education of Spain through research grant BIA2011-27217 is gratefully acknowledged. The company IGEOTEST has also partly supported this research.

REFERENCES

[1] ARROYO M., BUTLANSKA J., GENS A., CALVETTI F., JAMIOLKOWSKI M., *Cone penetration tests in a virtual calibration chamber*, Gèotechnique, 2011, 61(6), 525–531, DOI: 10.1680/geot.9.P.067.

[2] ARROYO M., BUTLANSKA J., GENS A., O'SULLIVAN C., *The effect of radial walls on CPT in a DEM-based virtual calibration chamber*, Third International Symposium on Computational Geomechanics (ComGeo III), Kraków, Poland, 21–23 August, 2013.

[3] BUTLANSKA J., ARROYO M., GENS A., *Homogeneity and symmetry in DEM models of cone penetration*, Proc. AIP Conf. on Powders and Grains, 2009, 1145, 425–429.

[4] BUTLANSKA J., ARROYO M., GENS A., (2010a), *Size effects on a virtual calibration chamber*, Numerical Methods in Geotechnical Engineering: NUMGE 2010, 2010a, 225–230.

[5] BUTLANSKA J., ARROYO M., GENS A., *Virtual Calibration Chamber CPT tests on Ticino sand*, Proc. 2nd International Symposium on Cone Penetration Testing, CPT'10, Huntington beach, California, Robertson & Mayne (eds.), 2010b, Vol. 2, 217–224.

[6] CUI L., O'SULLIVAN C., O'NEILL S., *An analysis of the triaxial apparatus using a mixed boundary three-dimensional discrete element model*, Gèotechnique, 2007, 57(10), 831–844, DOI: 10.1680/geot.2007.57.10.831.

[7] CUNDALL P.A., STRACK O.D.L., *A discrete numerical model for granular assemblies*, Gèotechnique, 1979, 29(1), 47–65, DOI: 10.1680/geot.1979.29.1.47.

[8] LIN J., WU W., *Numerical study of miniature penetrometer in granular material by discrete element method*, Philosophical Magazine, October 2012, 92(28–30), 3474–3482.

[9] Itasca, PFC3D Particle flow code in three dimensions V3.1 User Guide, Minneapolis: Itasca Consulting Group, 2005.

[10] MARKETOS G., BOLTON M.D., *Flat boundaries and their effect on sand testing*, Int. J. Numer. Anal. Meth. Geomech., 2010, 34, 821–837.

[11] MCDOWELL G., FALAGUSH O., YU H.S., *A particle refinement method for simulating DEM of cone penetration testing in granular materials*, Géotechnique Letters, 2012, 2, 141–147, http://dx.doi.org/10.1680/geolett.12.00036.